# Electronic Structure and Bonding in $YTi_2Ga_4$ – A Gallide with Linear Titanium Chains and Four-bonded Gallium Atoms

Samir F. Matar[a,b] and Rainer Pöttgen[c]

[a] CNRS, ICMCB, UPR 9048, 33600 Pessac, France
[b] Université Bordeaux, ICMCB, UPR 9048, 33600 Pessac, France
[c] Institut für Anorganische und Analytische Chemie, Universität Münster, Corrensstrasse 30, 48149 Münster, Germany

Reprint requests to S. F. Matar. E-mail: matar@icmcb-bordeaux.cnrs.fr

*Z. Naturforsch.* **2013**, *68b*, 23 – 28 / DOI: 10.5560/ZNB.2013-2299
Received November 22, 2012

The gallium-rich ternary intermetallic compound $YTi_2Ga_4$ is isotypic with $YbMo_2Al_4$, *I*4/*mmm*, $Z = 2$. Yttrium is located in a large cage built up by 12 gallium atoms. Chains of condensed $Y@Ga_{12}$ polyhedra and linear titanium chains build up a tetragonal rod packing. The gallium atoms are bonded within $Ga_4$ squares (265 pm Ga–Ga) which are condensed *via* longer Ga–Ga bonds (292 pm) to a three-dimensional gallium substructure with formally four-connected gallium, in agreement with a Bader charge partitioning scheme $[YTi_2]^{4+}[Ga_4]^{4-}$. These features are addressed with electronic structure and chemical bonding considerations. The metallic behavior of $YTi_2Ga_4$ is found to be of the itinerant electron type within the valence band and Ti *d*-like states at $E_F$. Ga–Ga and Ti–Ga bonding characteristics provide mechanical properties derived from the full set of elastic constants leading to a brittle material.

*Key words:* Gallide, Intermetallic Compound, Electronic Structure, Yttrium, Titanium

## Introduction

The aluminide $YbMo_2Al_4$ [1] crystallizes with its own structure type, space group *I*4/*mmm*, with peculiar substructures. The molybdenum atoms form linear chains which extend along the *c* axis, which are separated by $Al_4$ squares. $GdMo_2Al_4$ and $ErMo_2Al_4$ are isotypic with the ytterbium compound. This structure type has also been observed for a variety of gallides $RTi_2Ga_4$ ($R$ = Zr, Sc, Y, Tb, Dy, Ho, Er, Tm, Lu) [2 – 6] and $RV_2Ga_4$ ($R$ = Sc, Zr, Er, Hf) [2], the indide $SrAu_{4.76}In_{1.24}$ [7], the cadmium compounds $CaAu_4Cd_2$, $SrAu_4Cd_2$, and $EuAu_4Cd_2$ [8] as well as the solid solutions $YbCu_{5.1}Al_{0.9}$ [9], $YbCu_{5.12}Al_{0.88}$ [10] and $CeCu_{4.7}Mn_{1.3}$ [11]. From the point of view of chemical bonding, the coloring (*i. e.* exchanging the transition metal and *p*-element positions) of the polyanionic network is an interesting question, regarding *e. g.* $YbMo_2Al_4$ *vs.* $SrAu_4Cd_2$; aluminides *vs.* aurides *etc*.

In continuation of our studies on the structural data and chemical bonding behavior of $YbMo_2Al_4$ type intermetallics [7, 8] we have now investigated the electronic structure of $YTi_2Ga_4$ [4]. The purpose of this work is to present further analyses of the electronic band structure and the chemical bonding using computational methods built within the well-established quantum-theoretical density functional theory (DFT) framework [12, 13]. Two complementary computational methods were used. The Vienna *ab initio* simulation package (VASP) code with the PAW method [14, 15] allows geometry optimization, establishing the energy-volume equation of states EOS as well as the set of elastic stiffness constants and an analysis of the charge density. The full analysis of the electronic structure and the chemical bonding is then carried out using the full potential scalar-relativistic augmented spherical wave (ASW) method [16, 17]. The PBE generalized gradient approximation (GGA) functional [18], accounting for the effects of exchange and correlations within DFT, was considered in all calculations. For details of the methods the reader is referred to the theoretical development presented in ref. [19].

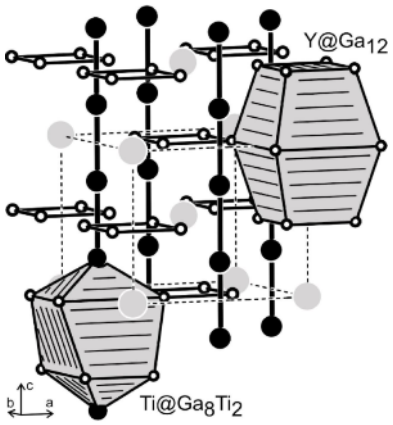


Fig. 1. The crystal structure of $YTi_2Ga_4$. Yttrium, titanium and gallium atoms are drawn as medium grey, black filled and open circles, respectively. The coordination polyhedra around the yttrium and titatium atoms as well as the titanium chains and the $Ga_4$ squares are emphasized.

## Results

### *Crystal chemistry*

The crystal structure of $YTi_2Ga_4$ (*I*4/*mmm*, $Z = 2$) [4] is shown in Fig. 1. The striking substructures are linear titanium chains which extend in *c* direction. The Ti–Ti distances of 274 pm are remarkably short when compared with *hcp* titanium ($6 \times 290$ and $6 \times 295$ pm) [20] or the chains in $Ti_2In_5$ (300 pm) [21]. This is indicative of substantial Ti–Ti bonding. The titanium chains are separated by $Ga_4$ squares with Ga–Ga distances of 265 pm, similar to those in the crystals of the element ($1 \times 244$ and $6 \times 270$ pm) [20]. Each titanium atom has two titanium neighbors within its chain and eight gallium neighbors at 279 pm Ti–Ga, somewhat longer than the sum of the covalent radii of 257 pm [22]. These $Ti@Ga_8Ti_2$ polyhedra interpenetrate each other along the *c* axis. Each titanium atom within a chain is a center of such a polyhedron. The yttrium atoms have twelve gallium neighbors at Y–Ga distances ranging from 288 to 332 pm. These $Y@Ga_{12}$ polyhedra are condensed *via* common square faces along the *c* axis. Since the $Y@Ga_{12}$ polyhedra comprise all gallium atoms in their coordination shell, we can alternatively describe the $YTi_2Ga_4$ structure as a tetragonal packing of rods of consensed $Y@Ga_{12}$ polyhedra and linear titanium chains. The peculiar features of chemical bonding are addressed in detail below.

### *Geometry optimization, equation of state and elastic modules*

Table 1 provides the experimental and calculated (in parentheses) structural parameters for $YTi_2Ga_4$. There is a good agreement for the gallium *x* coordinate (Wyckoff site 8*h*) but the geometry-optimized *a* and *c* parameters are calculated larger, respectively smaller, than the experimental ones, leading to a larger calculated cell volume of 0.1251 $nm^3$ per formula unit (fu) *versus* $V_{exp} = 0.1235\ nm^3$ per fu. This follows from the trend usually observed for the GGA DFT functional which is known to be underbinding, *i. e.* overestimating lattice spacing. Nevertheless the agreement is good enough to examine the physical properties such as the mechanical characteristics. One derives the equilibrium zero pressure parameters from the energy-volume, $E(V)$, equation-of-state (EOS) with calculations around minima found from geometry optimization. The resulting values are plotted in Fig. 2. The fit of the curves with a Birch EOS [23]:

$$E(V) = E_0(V_0) + [9/8]V_0B_0\left[([(V_0)/V])^{2/3} - 1\right]^2 + [9/16]B_0\left(B' - 4\right)V_0\left[([(V_0)/V])^{2/3} - 1\right]^3$$

provides $E_0$, $V_0$, $B_0$, and $B'$, respectively. The equilibrium energy, the volume, the bulk modulus and its pressure derivative are given in the inset. The fitted curves reproduce the trends of the geometry optimization for the volume. The corresponding zero pressure bulk modulus of $B_0 = 97$ GPa places the title compound in the range of intermetallics [24] which are softer than typical oxides and ceramics.

We also determined the elastic properties by performing finite distortions of the lattice and deriving the elastic constants from the strain-stress relationship. In tetragonal symmetry there are six independent elastic stiffness constants $C_{11}$, $C_{33}$, $C_{44}$, $C_{66}$, $C_{12}$, and $C_{13}$. Most samples are polycrystalline, where monocrystalline grains are randomly oriented so that on a large

Table 1. Experimental [4] and calculated (in parentheses) lattice and atomic parameters for $YTi_2Ga_4$, space group *I*4/*mmm*: $a = 671.2$ pm (677 pm), $c = 548.4$ pm (546 pm); Total energy per formula unit (fu): – 37.38 eV.

| Atom | Wyckoff site | *x* | *y* | *z* |
|---|---|---|---|---|
| Y | 2*a* | 0 | 0 | 0 |
| Ti | 4*d* | 0 | 1/2 | 1/4 |
| Ga | 8*h* | 0.303 (0.302) | *x* | 0 |

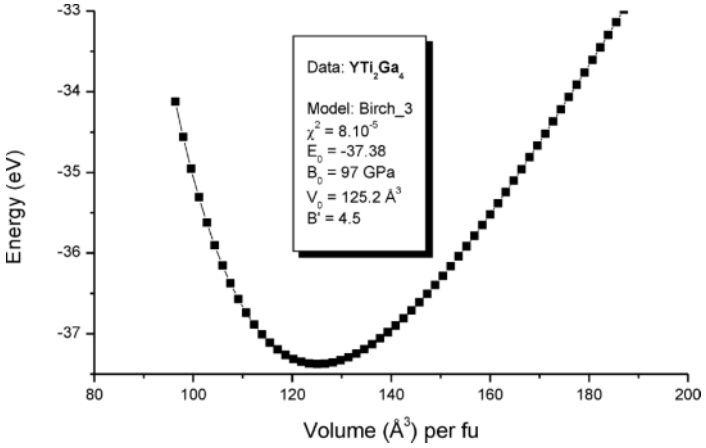


Fig. 2. $YTi_2Ga_4$: Energy volume curve and fit values (in the inset) from a Birch 3rd order equation of state.

scale such materials can be considered as statistically isotropic. They are then completely described by the bulk modulus B and the shear modulus G, which may be obtained by averaging the single-crystal elastic constants. The most widely used averaging procedure for the elastic stiffness constants is Voigt's method [25] based on a uniform strain. The calculated set of elastic constants in $YTi_2Ga_4$ in units of GPa are:

$$C_{11} = C_{22} = 175;\ C_{12} = 77;\ C_{13} = 55;$$
$$C_{33} = 160;\ C_{44} = 99 \text{ and } C_{66} = 53.$$

All $C_{ij}$ values are positive and their combinations: $C_{11} > C_{12}$, $C_{11}C_{33} > C_{13}^2$ and $(C_{11} + C_{12})C_{33} > 2C_{13}^2$ obey the rules pertaining to the mechanical stability of the intermetallic compound. The bulk ($B_V$) and shear ($G_V$) modules according to Voigt's method are formulated as:

$$B_V = 1/9\{2(C_{11} + C_{12}) + 4C_{13} + C_{33}\} \text{ and}$$
$$G_V = 1/30\{12C_{44} + 12C_{66} + C_{11} + C_{12} + 2C_{33} - 4C_{13}\}$$

The numerical values are then: $B_V = 98$ GPa and $G_V = 72$ GPa. The value of $B_V$ is in close agreement with the one obtained from the EOS fit (Fig. 2, inset) thus validating the two different approaches. The shear modulus which defines the rigidity of the material is significantly lower. The Pugh's $G/B$ ratio [26] is an indicator of brittleness or ductility for $G/B > 0.5$ and $G/B < 0.5$, respectively. For $YTi_2Ga_4$ $G/B = 0.73$, indicating brittleness, contrary to the properties of coinage metals Ag, Pt, or Au with $G/B$ ratios in the range of 0.4 – 0.2 [27]. This behavior should arise from directional bonding characteristics (*vide infra*).

*Analysis of charge transfer*

The analysis of the charge density issued from the self consistent calculations can be done using the AIM (atoms in molecules theory) approach [28] developed by Bader who devised an intuitive way of splitting molecules into atoms as based purely on the electronic charge density. Typically in chemical compounds, the charge density reaches a minimum between atoms, and this is the natural region to separate them from each other. Such an analysis can be useful when trends between similar compounds are examined; it does not constitute a tool for evaluating absolute ionizations. Bader's analysis is done using a fast algorithm operating on a charge density grid arising from high precision VASP calculations and generates the total charge associated with each atom. The results of computed charge changes ($\Delta Q$) are such that they lead to neutrality when the respective multiplicities are accounted for:

$$\Delta Q(\mathrm{Y}) = 1.376;\ \Delta Q(\mathrm{Ti}) = 1.315;\ \Delta Q(\mathrm{Ga}) = -1.$$

From these results one can formally write $[YTi_2]^{4+}[Ga_4]^{4-}$, thus classifying $YTi_2Ga_4$ as a gallide. According to this charge partitioning scheme the gallium components are formally isoelectronic with germanium, but we only observe two-connected gallium within the $Ga_4$ rings (265 pm Ga–Ga) instead of four-connected gallium. If we consider also the longer Ga–Ga distances of 292 pm between the

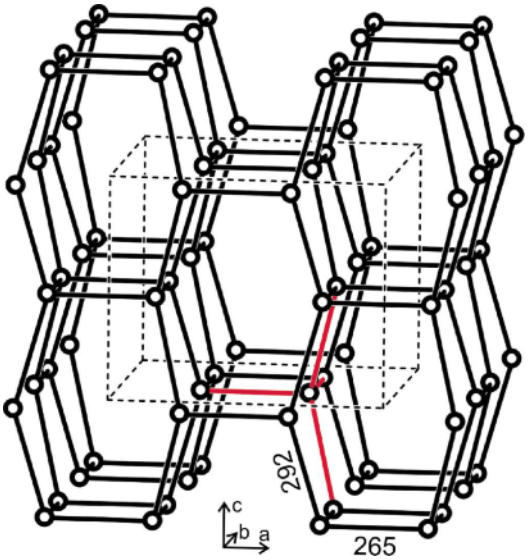


Fig. 3 (color online). The gallium substructure of $YTi_2Ga_4$. One distorted $Ga_4$ tetrahedron is emphasized in red color. Relevant interatomic distances are indicated.

$Ga_4$ rings, we obtain the three-dimensional gallium substructure (Fig. 3) which shows strongly distorted tetrahedral gallium coordination with Ga–Ga–Ga angles of 90, 104.1 (2×) and 139.7°. Thus, the $Ga^-$ entities formally fulfill Zintl's rule. Ideal $GaGa_{4/4}$ tetrahedra with 268 pm Ga–Ga distance occur in the NaTl-type Zintl phase LiGa [29]. $CaGa_2$ [30] contains elongated $GaGa_{4/4}$ tetrahedra with 265 and 306 pm Ga–Ga and Ga–Ga–Ga angles of 103.5 and 114.7°, comparable to the gallium substructure of $YTi_2Ga_4$. Nevertheless, $YTi_2Ga_4$ is not a Zintl phase in the classical sense. We observe strong covalent bonding of the gallium substructure with the titanium chains and pronounced metallic character.

The bonding peculiarities are further illustrated by the electron localization function (ELF). ELF is a normalized function ($0 \leq \mathrm{ELF} \leq 1$) [31, 32]. In the plots three main localization zones are identified: no localization for $\mathrm{ELF} = 0$ (blue areas), strong localization for 1 (red areas) and free electron like behavior for $\mathrm{ELF} = 1/2$ (green areas). The selected planes are shown in Fig. 4 for slices perpendicular to the tetragonal $c$ axis. The basal plane comprising two Ga and one Y (Fig. 4a) shows significant localization around the Ga atoms and an extension towards the intermediate plane (Fig. 4b). The red zones in the immediate surroundings of Y are due to the core electrons included in

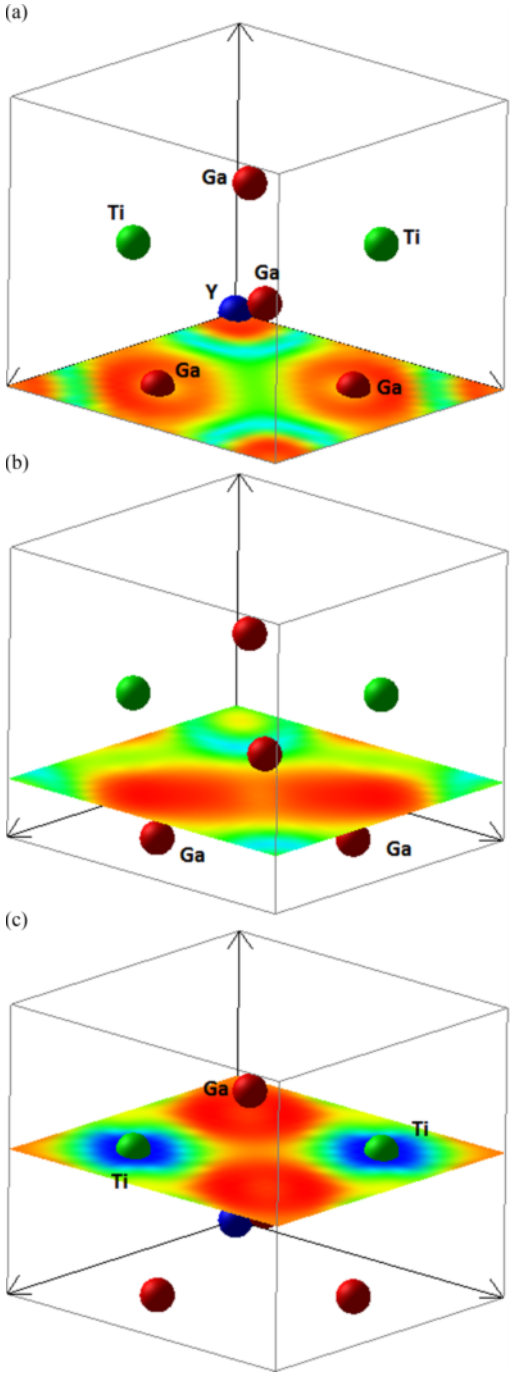


Fig. 4 (color online). $YTi_2Ga_4$: ELF slice planes perpendicular to the tetragonal $c$ axis. a) Basal plane comprising two Ga and one Y (at the origin); b) intermediate plane showing strong localization arising from the two gallium atoms at the basal plane and c) slice plane at $z = 1/2$ with titanium showing no localization ELF contours (*cf.* text).

the PAW method. The slice plane at $z = 1/2$ (Fig. 4c) contains Ti exhibiting no localization with blue ELF contours. The strong localization (ELF $\sim 1$) around Ga is more explicit than in the first panel and points to Ga–Ga bonding as shown in the next section.

*Electronic structure and chemical bonding*

Using the experimental structural data for $YTi_2Ga_4$ (Table 1) we analyze the electronic structure using all electron calculations with the full potential ASW method [16, 17]. The chemical bonding for pair interactions is analyzed qualitatively using the crystal orbital overlap populations COOP based on the overlap matrix elements $S_{ij}$ [33]. In the plots positive, negative and zero magnitude COOP indicate bonding, antibonding and non bonding interactions, respectively.

At self-consistent energy and charge convergence the transfer of electrons follows the trend discussed above. The site projected densities of states (PDOS) are shown in Fig. 5. The zero energy along the $x$ axis is with respect to the Fermi level $E_F$. The compound is metallic with mainly $d$-like PDOS arising from the lower part of Ti $d$ states. This is due to the low filling of the Ti $3d$ subshell with 2 electrons in the atomic state so that the $d$ band is centered above $E_F$ within the conduction band. The valence band from $-10$ eV up to $E_F$ is dominated by Ga $p$ states, and the valence band is mostly of itinerant $s, p$ like character. Similar PDOS shapes between Ga and Ti are noted for the lower part of Ti $d$ at $\sim -2$ eV, and quantum mixing can be expected leading to significant Ti – Ga bonding. Nevertheless, the similar PDOS shapes of Y and Ti just below $E_F$ indicate quantum mixing involving $d$ states.

Fig. 6 shows the COOP for the different interactions. The first panel (a) shows the COOP accounting for two atoms of each kind in order to allow comparisons of bond strengths. Clearly the Ga – Ga interaction is dominant and is found to be of bonding nature (positive COOP); it also reflects the Bader charge trends as well as the ELF plots presented in the preceding section. Ti – Ti bonding is largly present in the DOS region where $d$ states are found, thus indicating that Ti – Ti interaction along the chains is ensured by $d$ orbitals. This also follows the course of the dis-

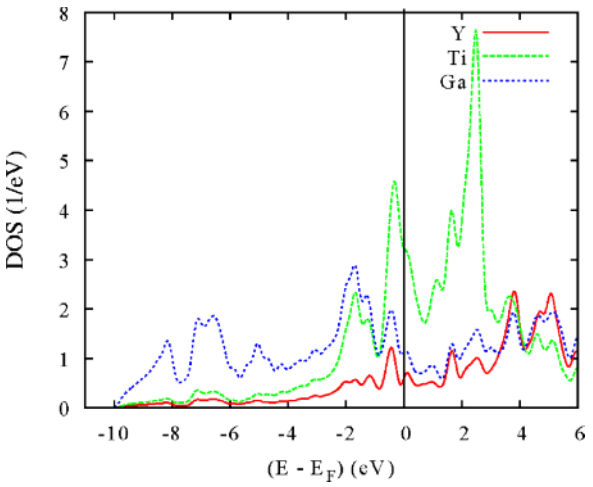


Fig. 5 (color online). $YTi_2Ga_4$: Site projected density of states (PDOS).

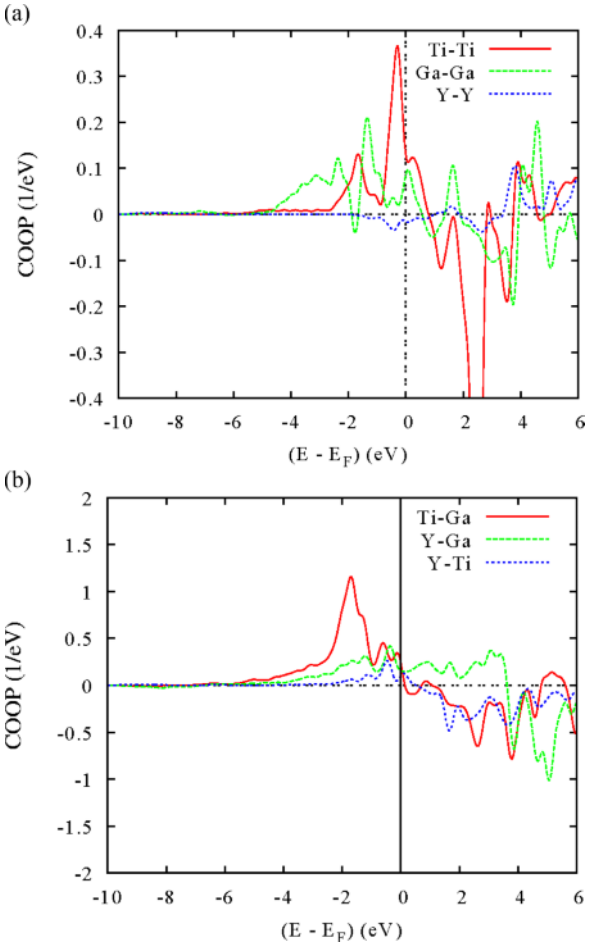


Fig. 6 (color online). $YTi_2Ga_4$: Chemical bonding according to the COOP criterion: a) for atoms of the same type, b) for atoms of different types.

tances whereby short Ti – Ti ($d_{Ti-Ti} = 274$ pm) connections are identified. Similar bonding characteristics were computed for $Hf_2In_5$ with Hf – Hf chains [34]. The titanium chains in the $RETi_2Ga_4$ gallides are non-magnetic. Temperature-dependent susceptibility measurements on samples with $RE$ = Tb – Er [5] reveal only the paramagnetic contribution of the $RE^{3+}$ ions.

Fig. 6b shows the bonding between the different chemical species accounting for their respective site multiplicities (Table 1). Strong bonding is observed for Ti – Ga, followed by the (much smaller) Y – Ga and Y – Ti COOPs which are vanishingly small except in the vicinity of $E_F$ involving the $d$ bands from both Y and Ti. The relative bonding strengths follow the course of the distances (in pm): $d_{Ga-Ga} = 265$; $d_{Ti-Ga} = 279$ and $d_{Y-Ga} = 288$.

The directional Ga – Ga and Ti – Ga interactions provide brittle mechanical properties as confirmed by the analysis of the elastic constants.

*Acknowledgement*

This work was supported by the Deutsche Forschungsgemeinschaft. Parts of the computations were conducted on the MCIA-University of Bordeaux computers.

[1] M. L. Fornasini, A. Palenzona, *J. Less-Common Met.* **1976**, *45*, 137.
[2] Y. Grin, I. S. Gavrilenko, V. Y. Markiv, Y. P. Yarmoluyk, *Dopov. Akad. Nauk Ukr. RSR, Ser. A* **1980**, 73.
[3] V. Y. Markiv, *Dopov. Akad. Nauk Ukr. RSR, Ser. A* **1981**, 86.
[4] V. Y. Markiv, T. G. Zhunkivska, N. M. Velyavina, O. O. Lisenko, *Dopov. Akad. Nauk Ukr. RSR, Ser. A* **1983**, 81.
[5] K. Gosh, S. Ramakrishnan, G. Chandra, *J. Magn. Magn. Mater.* **1993**, *119*, L5.
[6] H. Abe, K. Yoshii, H. Kitazawa, *J. Phys. Soc. Jpn.* **2001**, *70*, 3042.
[7] I. Muts, S. F. Matar, U. Ch. Rodewald, V. I. Zaremba, R. Pöttgen, *Z. Naturforsch.* **2011**, *66b*, 993.
[8] F. Tappe, S. F. Matar, C. Schwickert, R. Pöttgen, *Monatsh. Chem.* **2013**, *144*, submitted for publication.
[9] B. M. Stel'makhovych, Y. B. Kuz'ma, L. G. Akselrud, *Russ. Metall.* **1993**, *1*, 173.
[10] B. M. Stel'makhovych, Y. B. Kuz'ma, V. S. Babyzhet'sky, *J. Alloys Compd.* **1993**, *190*, 161.
[11] P. Manfrinetti, M. L. Fornasini, D. Mazzone, S. K. Dhar, R. Kulkarni, *J. Alloys Compd.* **2004**, *379*, 64.
[12] P. Hohenberg, W. Kohn, *Phys. Rev.* **1964**, *136*, B864.
[13] W. Kohn, L. J. Sham, *Phys. Rev.* **1965**, *140*, A1133.
[14] G. Kresse, J. Furthmüller, *Phys. Rev. B* **1996**, *54*, 11169.
[15] G. Kresse, J. Joubert, *Phys. Rev. B* **1999**, *59*, 1758.
[16] A. R. Williams, J. Kübler, C. D. Gelatt Jr., *Phys. Rev. B* **1979**, *19*, 6094.
[17] V. Eyert, V. *The Augmented Spherical Wave Method – A Comprehensive Treatment*, in *Lecture Notes in Physics*, Springer, Berlin, Heidelberg, **2007**, chapter 719.
[18] J. Perdew, K. Burke, M. Ernzerhof, *Phys. Rev. Lett.* **1996**, *77*, 3865.
[19] S. F. Matar, *Prog. Solid State Chem.* **2010**, *38*, 1.
[20] J. Donohue, *The Structures of the Elements*, Wiley, New York **1974**.
[21] R. Pöttgen, *Z. Naturforsch.* **1995**, *50b*, 1505.
[22] J. Emsley, *The Elements*, Oxford University Press, Oxford **1999**.
[23] F. Birch, *J. Geophys. Res.* **1978**, *83*, 1257.
[24] S. F. Matar, B. Chevalier, R. Pöttgen, *Intermetallics* **2012**, *31*, 88.
[25] S. F. Matar, *Matériaux ultra-durs: Concepts et Modélisations*. Série *Techniques de l'ingénieur,* Vol. AF 6630, T. I. Sciences et Techniques, Paris, **2009**.
[26] S. F. Pugh, *Phil. Mag.* **1954**, *45*, 823.
[27] S. Kamran, K. Chen, L. Chen, L. Zhao, *J. Phys.: Condens. Matter.* **2008**, *20*, 085221.
[28] R. Bader, *Chem. Rev.* **1991**, *91*, 893.
[29] E. Zintl, C. Brauer, *Z. Phys. Chem. (Abt. B)* **1933**, *20*, 245.
[30] W. Harms, M. Wendorff, C. Röhr, *Z. Naturforsch.* **2006**, *62b*, 177.
[31] A. D. Becke, K. E. Edgecombe, *J. Chem. Phys.* **1990**, *92*, 5397.
[32] B. Silvi, A. Savin, *Nature* **1994**, *371*, 683.
[33] R. Hofmann, *Angew. Chem. Int. Ed. Engl.* **1987**, *26*, 846.
[34] R. Pöttgen, R. Dronskowski, *Chem. Eur. J.* **1996**, *2*, 800.